Study of Pollutant Transport in Depth-averaged Flows using Random Walk Method

WU Xuefei
School of Environment and Resource, Southwest University of Science and Technology, Mianyang, China, Email: wuxf@swust.edu.cn

LIANG Dongfang
Department of Engineering, University of Cambridge, Cambridge, UK

Abstract: The random walk particle tracking (RWPT) method is compared with one of the Eulerian methods in investigating pollutant transport in depth-averaged flows. As a distinguished representative of Eulerian model with high performance, the MacCormack scheme with Total Variation Diminishing modification (TVD-MacCormack) is selected for comparison. Solute concentration is simulated. First, both numerical models have been tested by two idealized cases and compared against analytical solutions. Numerical dissipation is observed for TVD-Mac model where the concentration changes abruptly, especially under the circumstances of low resolution and disalignment between the flow direction and grid orientation. On the contrary, simulations by the random walk model achieve higher accuracy for both cases and is free of fictitious oscillations in the vicinity of sharp concentration gradients. Then, the solute oscillation along a one-dimensional hypothetical tidal estuary is simulated, showing RWPT accurately conserving mass and suffering less numerical diffusion compared with the Eulearian methods. Finally, the process of pollutant transport at the Yangzte River reach is predicted by RWPT. The longitudinal dispersion coefficient D_L is calculated accordingly. It is compared against that by theoretical/empirical formulae and the difference is in acceptable level, indicating the validity of RWPT in solving complex natural problems.

Key words: Mass transportation; Depth-averaged flow; Random walk particle tracking; TVD-MacCormack; Compare.

1. Introduction

In the wake of environment awareness and the following need to predict and improve the water quality in various of water bodies, increasing mathematical models have been developed for water pollution [1][2]. Generally, these models for mass transportation are classified into either Eulerian or Lagrangian methods. To date, most of researches are based on Eulerian solutions of the standard advection-diffusion equation using finite-difference or finite-element techniques [3][4]. These grid-based models, however, suffer from several drawbacks, such as the inaccuracy in resolving steep concentration gradients, and the inefficiency when the contaminants occupy only a small part of the calculation domain. On the contrary, Lagrangian methods offer a better solution to such problems. The random walk particle tracking model (RWPT) is one of the most popular representatives of such Lagrangian methods. RWPT utilizes a large number of discrete massless particles to represent the pollutant cloud that are released into the flow. Then all the particles are tracked independently. Hence, by definition, RWPT is perfectly mass conservative and free from artificial diffusion in the vicinity of steep concentration gradients. Also, as the computation in RWPT is limited to the region that the pollutant reaches, it is regarded as more computational efficient when dealing with blank area. Especially for advection-dominated problems, where Eulerian methods typically suffer from excessive numerical dispersion and artificial oscillation, RWPT offers a suitable alternative to the conventional methods [5].

Various numerical algorithms have been applied to the transport problems using Eulerian methods. Van Leer [6] introduced the Monotone Upstream-centred Scheme (MUSCL) and improves the computing of fluxes between grid cells. Benkhaldoun et al. [7] described the development of a non-homogeneous Riemann solver for pollutant transports by shallow water flows; Mingham et al.[4], and Liang et al. [3][8] applied a five-point TVD-MacCormack scheme to the depth-averaged transport equation. Liu et al. [9][10] used a sigma-coordinate water quality numerical model to simulate the process of both water and pollutant transportation in the trapezoidal channel open flow.

On the other hand, the Lagrangian methods are much less widespread. Liang [11] used RWPT to study the longitudinal dispersion processes in open channel flows in the presence of submerged vegetations. Barber [12] proposed a particle-tracking algorithm that can be used with arbitrary non-orthogonal boundary-fitted coordinate systems. And he proved the capabilities of the model by simulating wind-induced circulation and pollutant transport within the Gulf of Thermaikos, a semi-enclosed bay close to the City of Thessaloniki in northern Greece. Perianez [13] also applied the particle-tracking model to simulate the dispersion of contaminants in the Strait of Gibraltar.

Besides, still very little comparison has been made between RWPT and the conventional Eulerian method. In this paper, two idealized cases as well as a hypothetical tidal estuary were first simulated by RWPT, which is a Lagrangian approach. Through the comparison with that by the TVD-Mac model, a popular presentative of Eulerian methods [14], the advantage of the RWPT has been clearly revealed. RWPT is also used to simulate the motion of a contaminant cloud in a hypothetical tidal estuary, where extensive wetting and drying occurs with the tidal oscillation. The simulation result was compared with that by the TVD-Mac model [14] and displays comparatively higher accuracy and less numerical diffusion. Finally, the longitudinal dispersion coefficient D_L at the Yangzte river reach in China was calculated by RWPT. The development of D_L along travel time agree with that by several representatives of empirical/theoretical formulae at an acceptable level. Therefore, the model is also proved to be valid in solving the solute transport problems in a complex natural aquatic environment

2.Mass transportation in shallow water

The distribution of a substance in a fluid is governed by the advection-diffusion, assuming that the solute material exactly follows the flow. In this paper, calculation focuses on the depth-averaged cases, hence the depth-averaged solute transport equation Eq. (1), which considers advection, diffusion and reaction, is applied:

$$\frac{\partial(cd)}{\partial t}+\frac{\partial(ucd)}{\partial x}+\frac{\partial(ucd)}{\partial y}=\frac{\partial}{\partial x}\left(dD_{xx}\frac{\partial c}{\partial x}+dD_{xy}\frac{\partial c}{\partial y}\right)+\frac{\partial}{\partial y}\left(dD_{yx}\frac{\partial c}{\partial x}+dD_{yy}\frac{\partial c}{\partial y}\right)+q_s \qquad (1)$$

where c is the depth-averaged concentration of a solute, d is water depth, t is time, u and v are the velocity components along the two Cartesian coordinates, x and y, respectively, and D_{xx}, D_{xy}, D_{yx} and D_{yy} constitute the dispersion-diffusion tensor of depth-averaged mixing in Cartesian coordinates, which can refer to Fischer [15]. The last term q_s, representing the source/sink contribution per unit area, may be due to the waste water disposal throughout falls, pollutant decay/growth, chemical and biological transformations or a combination of these processes. $q_s > 0$ means the increase of pollutant, while $q_s < 0$ means that pollutant is destroyed and decreased.

The flow field with velocities is fed in the random walk model as the input. Together with the water depth, mixing coefficients, the two-dimensional model can then be conducted according to the depth-averaged random walk scheme described in the next section.

3. Depth-averaged random walk scheme

Following the method outlined by Józsa [16], the advection-diffusion equation is recast in a form that utilizes a particle-tracking algorithm. This is accomplished by introducing a new concentration variable: $C = cd$. Here, the sink/source term in Eq. (1) is neglected during derivation for brevity. Besides, the sink/source term can be included into the model by adding more particles, or assigning to every particle a variable pollutant mass, both of which may develop in time [17]. After algebraic manipulation, the depth-averaged advection-diffusion equation can be written as

$$\frac{\partial C}{\partial t}+\frac{\partial(UC)}{\partial x}+\frac{\partial(VC)}{\partial y}=\frac{\partial^2(D_{xx}C)}{\partial x^2}+2\frac{\partial^2(D_{xy}C)}{\partial x\partial y}+\frac{\partial^2(D_{yy}C)}{\partial y^2} \qquad (2)$$

Where

$$U=u+\frac{\partial D_{xx}}{\partial x}+\frac{\partial D_{xy}}{\partial y}+\frac{D_{xx}}{d}\frac{\partial d}{\partial x}+\frac{D_{xy}}{d}\frac{\partial d}{\partial y} \qquad (3a)$$

$$V = v + \frac{\partial D_{yy}}{\partial y} + \frac{\partial D_{xy}}{\partial x} + \frac{D_{yy}}{d}\frac{\partial d}{\partial y} + \frac{D_{xy}}{d}\frac{\partial d}{\partial x} \tag{3b}$$

We consider the concentration, *C*, as a probability density function, then Eq. (2) is identical to the Fokker-Planck equation. The modified advective velocities in Eq.(3a) and Eq.(3b) allow the particle-tracking scheme to simulate diffusion using a consistent random-walk technique.

Then, the random walk model is carried out by two processes: the advective transport and the diffusive transport for each time step.

3.1 Advective transport

As most of the input flow field is solved by a grid-based method, it is necessary to evaluate the advective velocities in Eq.(3a) and Eq.(3b) at each particle's position, in order to transport the particles due to pure advection. The advective velocities, *u* and *v*, are computed using Taylor series expansions up to second-order about the nearest non-zero velocity node in the grid cell containing the particle.

Now the interpolated velocities of the particle can be substituted into Eq.(3a) and Eq.(3b) to get the modified advective velocities. Then the new particle position due to advection is:

$$x_a\left(t+\Delta t\right) = x_a\left(t\right) + U_a \Delta t \tag{4a}$$

$$y_a\left(t+\Delta t\right) = y_a\left(t\right) + V_a \Delta t \tag{4b}$$

Here, a second-order accurate iterative technique is used to calculate U_a, V_a, as they are the mean velocity during one time step, hence being taking as the average of the velocity before and after advection.

3.2 Diffusive transport

Following the advective stage in one time step, the particles are then subjected to diffusion. This is where the random velocity components are added. The random parts of the longitudinal and transverse velocities are generated as

$$u_d^L = r_1\sqrt{\frac{2D_l}{\Delta t}} \tag{5a}$$

$$u_d^T = r_2\sqrt{\frac{2D_t}{\Delta t}} \tag{5b}$$

where r_1 and r_2 are independent normally distributed random numbers with zero mean and standard deviation of unity. As the diffusive velocities are calculated in longitudinal and transverse, they must be expressed in terms of the Cartesian coordinate system by transformation such that

$$U_d = u_d^L \cos\theta - u_d^T \sin\theta \tag{6a}$$

$$V_d = u_d^L \sin\theta + u_d^T \cos\theta \tag{6b}$$

Therefore, the final x and y coordinates of the particle after one-time step can be expressed as

$$x_{new} = x_a\left(t+\Delta t\right) + U_d \Delta t \tag{7a}$$

$$y_{new} = y_a\left(t+\Delta t\right) + V_d \Delta t \tag{7b}$$

Inside the calculation domain, the particles follow a "random walk" path with the flow, as dictated by the above equation. At boundaries, however, special treatments are needed to prevent them from crossing the boundaries. The water surface and the channel bottom are regarded to act as reflective mirrors. Particles crossing them would be reflected back into the domain. Hence mass conservation is maintained. More detailed treatment to the more complex boundary will be discussed in section 4.

According to the above procedures, the position of every particle at every time step can be tracked. By analyzing the statistics of the positions of a large number of particles, the longitudinal dispersion coefficient D_L can be determined. D_L is often used to represent the mixing rate, which has become a key parameter in water-quality modeling. After a certain time since the release of the particle ensemble, known as the Fickian time, the standard deviation of particles' positions in the longitudinal direction increases linearly with time, indicating that D_L converges to a constant. As a measure of the spatially-averaged spreading rate of a tracer cloud, D_L can be calculated according to the time change of the longitudinal variance of the particle ensemble

$$\mathrm{D}_L = \frac{1}{2}\frac{\sigma_x^2(t_2)-\sigma_x^2(t_1)}{t_2-t_1} \tag{8}$$

4Verification

In this section, two idealized test cases are selected to examine the performance of the random walk model. The model is also used to simulate the motion of a contaminant cloud in a hypothetical tidal estuary, where extensive wetting and drying occurs with the tidal oscillation. The numerical predictions are compared with analytical solutions and results by the TVD-MacCormack (TVD-Mac) scheme. The TVD-Mac scheme, which is an advanced Eulerian model, is based on the standard MacCormack scheme, with a five-point Total Variation Diminishing (TVD) modification. It is chosen as a representative for the Eulerian method, because compared with other classic Euler method, it not only displays sufficiently high efficiency and accuracy in solving the solute transport problems, but also maintains the mass balance and accurately treats the cross-diffusion terms in complex flow situations.

According to our experiments, the size of time step in steady flow was set reasonably large, since the size of time step has little impact on the accuracy of the random walk model in steady flow [18]. On the contrary, unsteady flow is sensitive to the size of the time step, thus a comparatively small size of time step must be applied in such cases. Then the particles number was chosen accordingly to achieve a balance between the computational cost and accuracy.

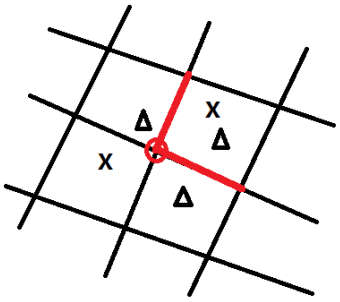

Fig. 1 A schematic diagram of the moving boundary treatment

Solution for the moving boundaries problem is also noteworthy. Moving boundaries are often caused by the varying water level in environmental flows. The wetting and drying phenomena are modeled by prescribing a minimum water depth H_{min}, below which the computational nodes are deemed to be dry and thus excluded in the subsequent computations. No flux conditions, in both the flow and solute computations, are enforced between the wet and dry nodes nor between the wet nodes and solid boundaries. As the random walk model is a mesh-free Lagrangian method, such nodes come from the Eulerian method for the calculation of flow fields, including water depth and velocity etc., which will be fed in as the input condition of RWPT. Over the dry nodes, the water depth and solute concentration are frozen to the values when the nodes are last wet to ensure mass balance. A wetting check is undertaken in each time step, where the water levels of the four nodes of the cell that the particle locates at, are all compared with H_{min}. There are different cases for which different treatments are launched accordingly: (i) If the water levels are higher than H_{min} for all the four nodes of the new cell that the particle travels to during this time step, then no additional treatment is needed, particles can travel totally free. (ii) If (i) does not stand (means the particle is traveling along the dry-wet boundary), then the boundary which the particle crossed during this time step will be considered as: (ii.a) the particle (Δ in Fig. 1) traveled across the dry-wet cell line, as illustrated by the red lines, then

the two dots on this line are double-checked: if none of them has a water level that is higher than H_{min}, then the particle will be frozen to the previous position; (ii.b) the particle (X in Fig. 1) traveled across a cell dot, as illustrated by the red circle, then a dry dot (water level lower than H_{min}) will stop the particle from traveling, i.e. particle will be frozen to the previous location; otherwise, the particle can move freely. In all the present simulations, H_{min} has been set to less than 2mm. Although this empirical treatment of the wetting and drying process does not follow strict mathematical derivations, it is physically sensible and has been shown to be reliable in practical simulations [19].

4.1 Advection and decay in a rotating flow field

The random walk model was first applied to simulate the movement of a circular patch of solute in a rotating flow field. Then the simulation result was compared with that by the TVD-Mac scheme [14]. The computational domain was contained inside a square, with a side of length 80*m*. The water body had a constant water depth of 1*m*, and the velocity field was steady and specified as follows:

$$u = -(y-40)\cdot\frac{2\pi}{360} \tag{9a}$$

$$v = -(x-40)\cdot\frac{2\pi}{360} \tag{9b}$$

Eq. (9) indicates that the water rotates counterclockwise about the center of the domain as a rigid body, and one rotation takes 360*s*. The domain was divided into grid cells with an equal spacing of 1*m*. Initially, the unit concentration was specified within a circle, which had a radius of 7*m* and was centered at $x = 20m$ and $y = 40m$, and the concentration elsewhere was zero, as illustrated in Fig.2a.

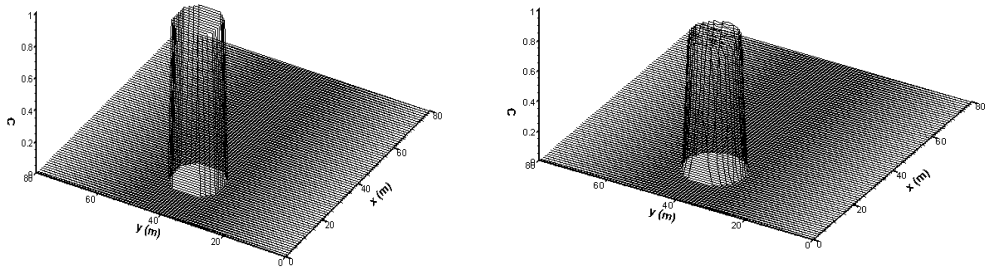

(a) Initial concentration **(b) Random walk results after one rotation t = 360s**

Fig. 2 Concentration in rotating flow

Neither the diffusion terms nor the sink/source term in Eq. (1) is included in this example. The predicted concentration distributions after one rotation by the random walk scheme is shown in Fig.2b. In this pure advection scenario, the circular column should theoretically return to its original position, with its original shape. However, it is extremely difficult to maintain with Eulerian methods, especially at the edge of the column where steep concentration gradient occurs. This is proved by the numerical diffusion shown in Fig. 3, 4, where the blue lines represent the simulated concentration by TVD-Mac. The shape of the column becomes asymmetrical as it rotates due to the variation of numerical diffusion in different directions and numerical dispersion. Although the TVD-Mac scheme, as an improved one compared with the standard MacCormack scheme, removes the numerical oscillations at the foot of the concentration column where abrupt changes take place. It still exhibits a certain degree of excessive numerical damping. In particular, more dissipation is experienced at the front face of the concentration column than in the other directions, as reflected by the more gradual decrease to zero in the direction where the column travels.

On the contrary, the prediction by the random walk scheme is totally free from the numerical oscillations and perfectly maintains the concentration along the whole way of rotation. Fig.3 presents the quantitative contrast between the simulation results by the TVD-Mac scheme (blue

lines), and the random walk model (red lines). As can be seen, the random walk model, compared against the exact solution, enjoys a much higher accuracy than that of the Euler method with much lass numerical diffusion.

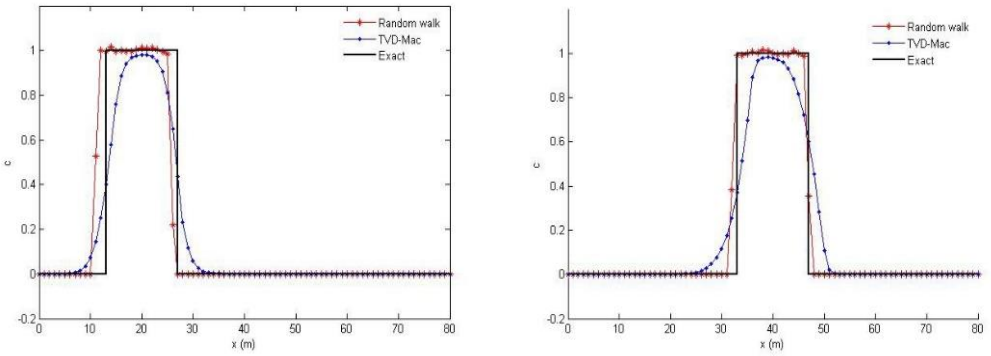

(a) Along line y = 40m **(b) along line x = 20m**

Fig. 3 Concentration variations after one rotation, t = 360s. (a) Along line y = 40m; (b) along line x = 20m

With the flow field and initial concentration distribution unchanged, the first-order decay of the contaminant is introduced by setting the source term q_S in Eq. (1) to be

$$q_s = -0.00447 \cdot c \tag{10}$$

Theoretically, the concentration column should maintain its shape but exponentially decrease its height. In Eq. (10), a coefficient of 0.00447 is chosen so that the maximum concentration will decrease from 1 unit at the beginning to 0.2 units at $t = 360s$. The quantitative comparisons of the simulations after one complete rotation are shown in Fig.4. It is seen that the previous conclusions still apply to this problem: comprising both advection and decay, the degree of numerical diffusion from the TVD-Mac scheme remains similar while the random walk model remains much closer to the exact solution.

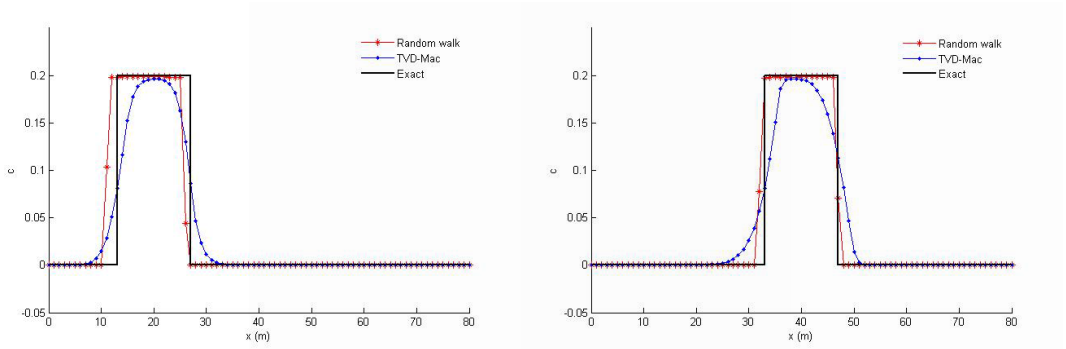

(a) Along line y = 40m **(b) along line x = 20m**

Fig. 4 Concentration variations after one rotation with decay. (a) Along line y = 40m; (b) along line x = 20m

4.2 Advection and diffusion in a uniform flow field

The instantaneous release problem in uniform flows was tested in this section, which involves both the advection and diffusion phenomena. The basic solution for this problem is acquired in an infinite domain. To eliminate boundary effects, the test domain extends from 0 to $800m$ in both the x and y directions. When the flow is along the x axis, i.e. $V = 0$ and $D_{xy} = 0$, the analytical solution can be formulated as

$$C(x, y, t) = \frac{M / d}{4\pi t\sqrt{D_{xx} D_{yy}}} \exp\left(-\frac{(x - x_0 - ut)^2}{4D_{xx} t} - \frac{(y - y_0)^2}{4D_{yy} t} \right) \tag{11}$$

where $M = 233.06$ is the total amount of solute or pollutant, the water depth is $d = 1m$, the velocity is

set to $u = 1m/s$, and $(x_0, y_0) = (0, 400m)$ is the location at which the sudden influx of mass takes place at $t = 0$. In the present study, the simulation starts from $t = 60s$. By fixing the Chezy coefficient at $40m^{1/2}/s$ and the longitudinal dispersion and lateral diffusion constants at 13.0 and 1.2 respectively, the mixing coefficients are calculated to be $D_{xx} = 1.02m^2/s$ and $D_{yy} = 0.094\ m^2/s$. It can be shown that this combination of values produces a peak concentration of unity at 60s after the release. For the Euler computation in this section, the grid size is 1m and the time step is 0.5s, while the particles number is 2.3e6 and time step is 1s for the random walk model.

The concentration contours are predicted to evolve as shown in Fig. 5a, where the concentration below 0.002 units is truncated for the clarity of visualization. As the magnitude of the longitudinal dispersion is more than ten times larger than that of the lateral diffusion, the cloud experienced rapid elongation in the flow direction. Such results apply to the simulations by both the TVD-Mac [14], and RWPT as Fig.5. Fig.5 is a qualitative illustration of the evolution of the pollutant cloud with time. The quantitative analyses are given in Fig.6, 7, where the simulations by the random walk model coincide well with the exact solution.

To verify whether the cross-diffusion terms are handled correctly in the model, the same phenomenon was simulated again with the flow aligned in the diagonal direction, i.e. $U = V = 1/\sqrt{2}\ m/s$. In order to make the center of the cloud reside at (x, y) = (60m, 60m) at t = 60s, the initial release location is set at (x_0, y_0) = (17.87m, 17.87m). The simulation results are illustrated in Fig. 5b.

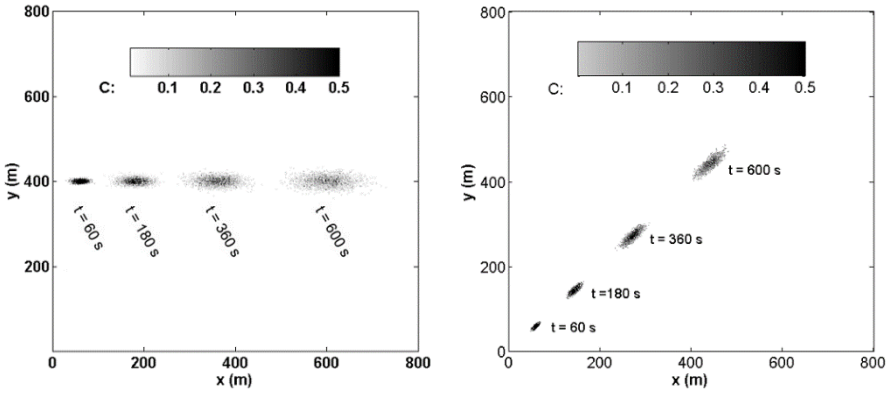

(a) in x direction **(b) in diagonal direction**

Fig. 5 Evolution of the pollutant cloud with time by RWPT

Visual inspection of the elliptical patches of solute distribution reveals a fairly good match between the two sets of results in x-direction flow and diagonal flow, with the major axis of the ellipses always in line with the flow direction, as shown in Fig 5.

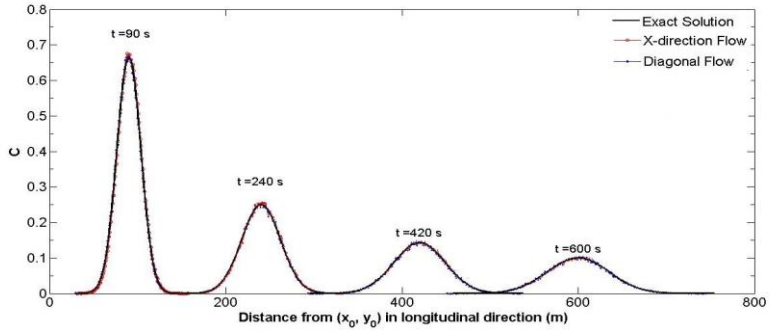

Fig. 6 Longitudinal concentration profile development

Quantitative comparisons between the predicted and analytical results are shown in Fig.6, 7. 8. Fig. 6 plots the concentration profiles in the streamwise direction at several instants. Fig.7 illustrates the decrease of peak concentration with time. It is seen that the simulated concentrations at various times are in perfect agreement with the analytical solution for both flows that is aligned in the x-direction and that is oriented in the diagonal direction. The peak concentration simulated by

the random walk model, as can be seen in Fig.7b, always identical with the analytical solution for both flows, too.

However, such a good agreement is not tenable for TVD-Mac. The simulation results by the TVD-Mac scheme shows the same good agreement with the analytical solution for the flow that is aligned in the x-direction; while for the flow which is oriented in the diagonal direction, the peak concentration is slightly under predicted, especially at an early stage of transport, as shown in Fig.7a.

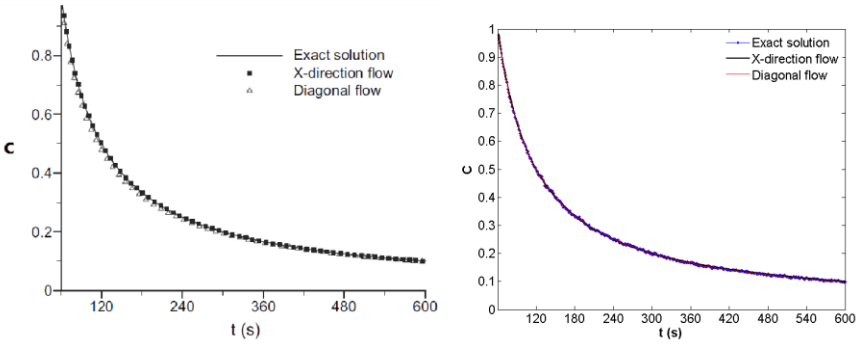

(a) TVD-MacCormack **(b) Random walk**

Fig. 7 Variation of peak concentration with time

Fig.8 illustrates the relative error of the simulated peak concentrations against the theoretical values. Fig.8a shows the relative error of the TVD-Mac scheme. In the diagonal flow, the relative error jumped to about 4% soon after the simulation started, and then decreased corresponding to the decrease of the concentration gradient. When the flow is aligned with the x-axis, the computational error is reduced by one order of magnitude. The predictions for the x-direction flow case are more accurate, which can be attributed to the simpler equation for such a configuration, i.e. Eq. (1) is simplified with $D_{xy} = 0$. For this grid-based method, some extra numerical damping is generated when the flow direction is not aligned with the grid orientation, and it becomes apparent when the variation is steep in the concentration field. In the studied example, the maximum concentration gradient occurs in the direction perpendicular to the flow. Therefore, another reason for the less satisfactory predictions in the diagonal flow is that the grid resolution in the cross-flow direction therein is poorer than that in the x-direction flow case.

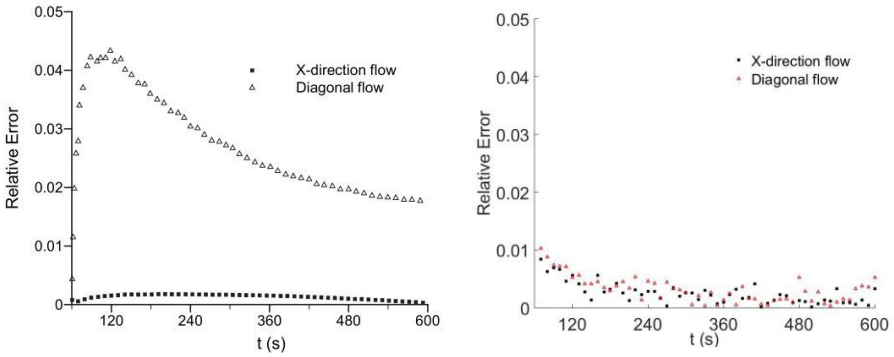

(a)TVD-MacCormack **(b)Random walk**

Fig. 8 Variation of relative error with time

On the contrary, the random walk model, as shown in Fig.9b, is totally free of such extra numerical damping from the grid orientation. Thanks to the grid-free nature of the random walk model, the simulation results can achieve the same level of accuracy despite the direction of the flow in the Cartesian coordinate. This can also be noted as an advantage of the random walk model over the TVD-Mac scheme.

4.3 Solute oscillation along hypothetical tidal estuary

In order to examine the ability of the present model in handling the moving boundaries and further compare with the Eulerian methods, this section considers water flow and solute transport in a one-dimensional estuary. The estuary was aligned in the x-direction with a length of 13,800 m. The bed elevation of the estuary changed from −5 m at the left (or seaward) end to 0 at the right (or landward)

end of the estuary, giving a uniform slope of 1 in 2760. The right end of the estuary was closed by a vertical wall, while a sinusoidal tide was fed in at the left end. The specified tide had a mean water level of 0, an amplitude of 2m, and it began to rise from mean water level at the beginning of the simulation. In total, five tidal cycles were simulated. The prediction of the flow field was achieved by solving the shallow water equations with the TVD-MacCormack scheme, details of which can be found in Liang et al. ([14]). Corresponding to the receding tide and rising tide, the right part of the computational domain underwent repetitive drying and wetting.

At the start of the simulations, the concentration all over the domain was set to zero except for one grid cell centered at x = 10 km, where the concentration was equated to 100 units. The dispersion constant was taken to be 13.0. Under the action of the tidal flows, this instantaneously released solute travels to the closed wall with the rising water and to the open boundary with the receding water. At the same time, the solute is dispersed to a larger region. The concentration cloud was found to move roughly to the rightmost position at high water and the leftmost position at low water. Because the tidal current generally decelerated when approaching the closed boundary, the center of the solute cloud moved a shorter length in the shoreward direction from the location of release than in the seaward direction. A series of concentration distributions at high and low water are plotted in Fig.9, which clearly illustrates the scattering of the solute with time.

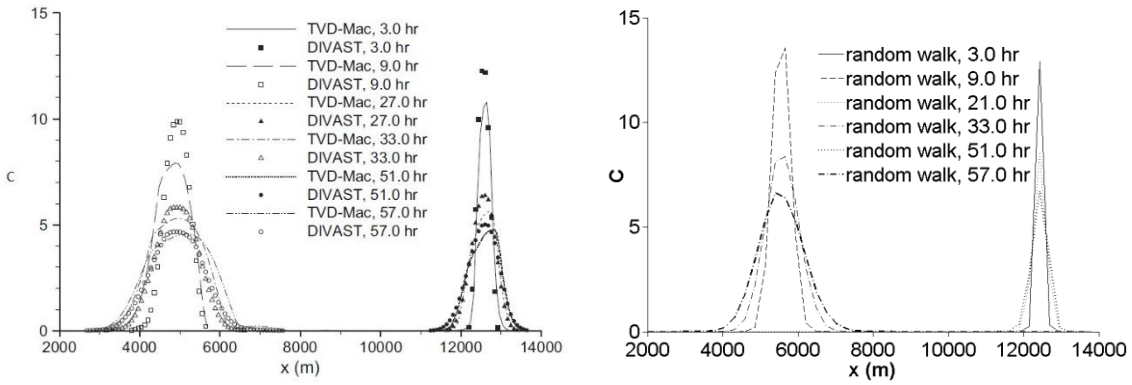

(a) TVD-Mac and DIVAST methods **(b) RWPT**

Fig. 9 Development of the concentration distribution along the hypothetical estuary

Fig.9 also shows the predictions made by different Eulerian models, including not only the TVD-Mac scheme, but also the DIVAST (Depth Integrated Velocities and Solute Transport) model, which solves the solute transport equation by the ULTIMATE QUICKEST scheme [20]. These two Eulerian methods are selected because both enjoy certain advantage while suffering from some other defect. In contrast, the random walk model can handle both sides well, which I will explain in detail as below.

First, owing to the sharp concentration gradient, the numerical diffusion for these Eulerian models can be quite large at the beginning, as shown in Fig.9a. The DIVAST model is less diffusive, so it predicts a narrower distribution with a higher peak concentration. However, the difference between the DIVAST and TVD-MacCormack models gets smaller and smaller as time progresses and it almost diminishes in the fifth tide.

On the other hand, the mass conservation, as one of the main weaknesses that Eulerian methods often confront, should be checked. Fig.9 shows that the solute cloud was still of some distance away from the open boundary on the left, even towards the end of the simulation. As no solute had escaped, the total amount of the solute within the domain should maintain the initially released value throughout the simulation. As shown in Fig.10, the TVD-MacCormack model conserved the mass perfectly; while the total amount of the solute simulated by the DIVAST model was higher than the exact value and exhibited the oscillation with a same period as the tide, although the deviation was within 1%.

In summary, the TVD-MacCormack scheme can conserve mass, but suffers from a larger numerical diffusion; on the contrary, the DIVAST model is less diffusive while has a fluctuation on total mass. Comparing with these Eulerian methods, the random walk model is not only always perfectly mass

conserving by its definition, as shown in Fig. 10, but also has less numerical diffusion, as can be seen in Fig.9b.

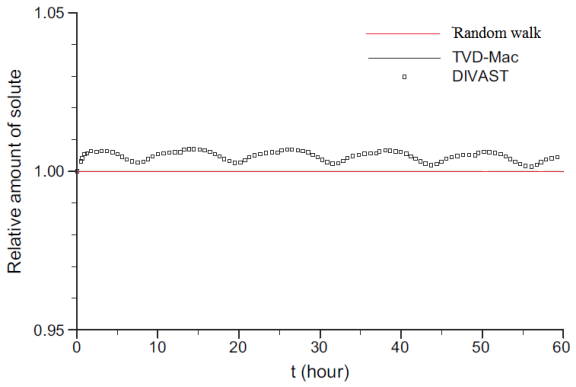

Fig. 10 Variation of the normalised total pollutant amount

5. Application – The Yangtze River Reach

The calculation domain in this section involves the Yangtze river reach between the Three Gorges dam and the Gezhouba dam. Both dams span the Yangtze River by Hubei province, China. Wherein the Three Gorges dam is the world's largest power station in terms of installed capacity. Fig.11 presents an overall top-view of the region (Fig.11a) and the local map with detailed indication of the two dams at upstream and downstream (Fig.11b).

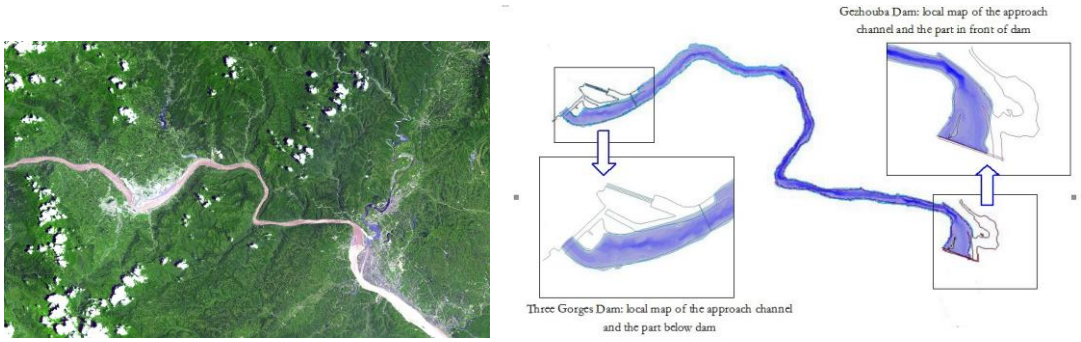

(a) Satellite map showing areas between the Three Gorges reservoir (left side) and the Gezhouba Dam reservoir (right side)

(b) local map illustrating the scope of the model

Fig. 11 Scope of the model for the reach between the Three Gorges Dam and the Gezhouba Dam

On the other hand, the pollution related to the hydraulic projects is getting more and more attention for its enormous potential influence. The pollutant transportation in this area is of immense importance not only to the projects themselves but also to the ambient environment. Quite a few investigations have been taken by domestic scholars as well as international academics [22][23]. However, most of the studies adopted Eulerian methods instead of the random walk model, which missed the great advantage of this Lagrangian approach. Besides, the long-slim-shaped terrain has a much more complicated grid for the flow field as the input condition. Hence this section also demonstrates the capacity of the random walk model on solving problems with irregular flow field grid.

5.1 Evaluate the longitudinal dispersion coefficient D_L by the random walk model

In natural rivers, such as the Yangtze river reach studied here, the longitudinal dispersion coefficient D_L is the most dominant dispersion component and is much larger than that in the two-dimensional idealized open channel flows. This is because the section profile, bed slope as well as the velocity vary greatly along the river, resulting in much larger dispersion on the pollutant. Therefore, it is a very important though extremely complicated task to evaluate D_L in such natural rivers.

Although it seems to be a long-slim-shaped terrain, the water depth along the river reach is at least one order of magnitude smaller than the width of the river. Therefore, the lateral shear is still the

dominating driving force for mass transport, thus the depth-integrated approach is again adopted in this case. Given the unsteady flow field at $t = 0hr$ and $t = 60hr$, as the input condition, the random walk model is applied to evaluate the longitudinal dispersion coefficient D_L using Eq. (8). Also, the longitudinal and lateral diffusion coefficients are determined with typical values of 13.0 and 1.2 for the longitudinal dispersion and turbulent diffusion constants ε_l, ε_t respectively.

A hypothetical release scenario is considered, where a substance is discharged instantaneously into the water body from the inlet part of the calculation domain. In this paper, line release was selected. We may also try out other initial conditions, such as point release, and the same scheme may apply. It is worth mentioning that, particles released at the "dry zones", where $H < H_{min}$, will be 'frozen' and thus not be considered in the subsequent calculation. Therefore, all the particles are released at the central part of the river, where water is deep enough to drive the particles. 100,000 particles are used, and the time step is set to be $1s$ in the simulation.

The travel process of the particles along the river at various times is presented in Fig. 12. As can be seen in these figures, especially in Fig. 12(a), particles travel faster in the middle of the river where larger flow velocity and deeper water occur. Because of the Gezhouba dam which blocks the particles from further traveling, particles gradually accumulate at the downstream side. Consequently, the variance of the particles distribution cannot develop freely but starts declining. Such phenomenon is confirmed and illustrated in Fig. 12(g) and Fig. 12(h), as much less travel progress can be seen during the five hours between these two panels than that occurs between any other five-hour-interval before. This well explains the decline of the longitudinal dispersion coefficient D_L at the later part of Fig.14, which shows the development of D_L along with time.

The concentration distributions along the river at different time are illustrated in Fig.13. The horizontal ordinate of the figure is the distance from inlet in longitudinal direction, rather than the x coordinates, indicating the travel distance of particles along the river; The vertical coordinates are the number of particles, which can be easily converted to concentration by Eq. (21)

$$c = N \cdot m / (WHL_{bin}) \tag{12}$$

where c and N represent the concentration and particles number at the location, respectively; m is the unit mass that one particle represents (although the effects from mass is ignored in calculation); W and H are the local width and depth of the river, respectively; L_{bin} is the bin-width when calculating the histogram.

As we know, the statistical equation Eq. (8) for the evaluation of D_L is valid only when the particles distribution becomes normal distribution. In Fig.13, the particles distributions in panels (a) - (f) are roughly normal, except for a few odd peaks which are indicated by the numbers from 1 to 5. At $t = 1h$, the particles follow skewed normal distribution, implying the Fickian limit has not been reached. Meanwhile, unlike the later distributions, there is no odd peak at this stage. This is because the particles have not reached the irregular terrain of the river. When particles pass the irregular terrain, as happened later, the distribution will be interfered, resulting in odd peaks in panels (b) - (h). Fig. 15(a) shows the locations at the river where the odd peak points in Fig.13 occur. The No.1 peak point in Fig.13 is due to the contraction of river width. Points 2 - 5 appear because these curve bends of the river have made a favorable condition for the suspension of particles.

Also, by comparing (b) and (c) in Fig. 13, it is noted that some particles travel backward, as marked by the red circle in (c). Such seemingly unreasonable phenomena can be explained by Fig. 15(b), where a back-flow takes place due to the contraction of river width and forms a large vortex. The last two figures (g) and (h) in Fig.13 present the distribution after $t = 30h$, which significantly deviate from the normal distribution. Together with Fig.12(g), (h), they have proved the accumulation of particles at the outlet due to the blockage of the Gezhouba dam, which also explained the decline of D_L in Fig.14 after $t = 25h$.

The simulated D_L by the depth-averaged two-dimensional random walk model is illustrated by Fig.21. Prior to the Fickian time, the front part of the figure, particles have not been well-mixed across the river section and differential advection dominates, resulting in a nonlinear increase of particles distribution variance. While the decrease of D_L at the later part of the figure, as explained before, is because of the blockage from the Gezhouba dam. The fluctuations in the middle are the results of the complex terrain along the river. The longitudinal dispersion coefficient D_L can be then

calculated as the average value during t = 10h to t = 25h. This period is selected first to safely satisfy the Fickian limit as well as avoid the blocked part at the end; secondly, the random walk model can present D_L along the passage of particles' traveling, hence reflecting the real-time local condition. However, an average value of D_L must be given in order to compare with D_L by empirical or theoretical formulae. Hence, we cut out a proper period to calculate the mean value.

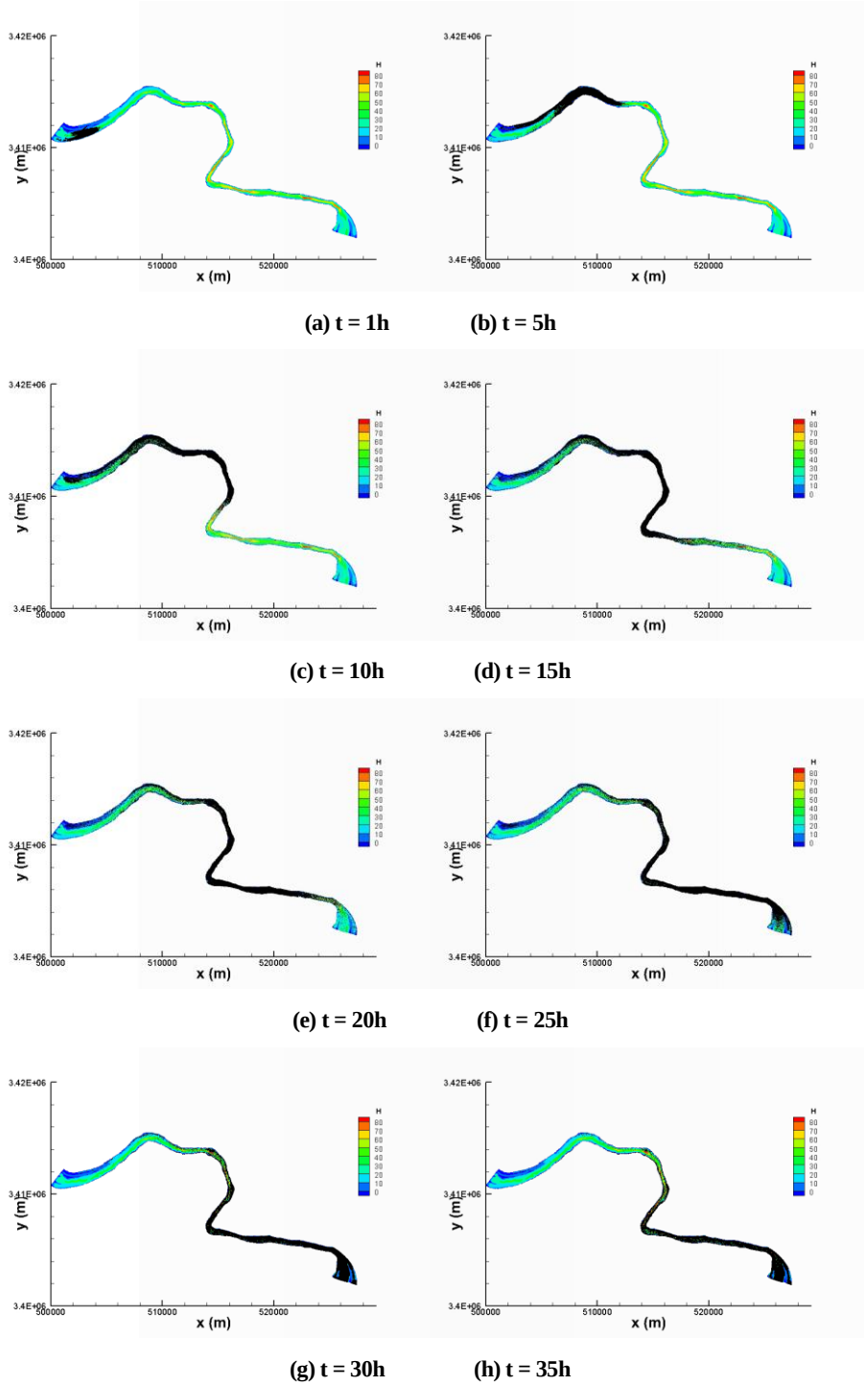

(a) t = 1h **(b) t = 5h**

(c) t = 10h **(d) t = 15h**

(e) t = 20h **(f) t = 25h**

(g) t = 30h **(h) t = 35h**

Fig. 12 Travel of the pollutant particles along the Yangtze river. (a) t = 1h, (b) t = 5h, (c) t = 10h, (d) t = 15h, (e) t = 20h, (f) t = 25h, (g) t = 30h, (h) t = 35h.

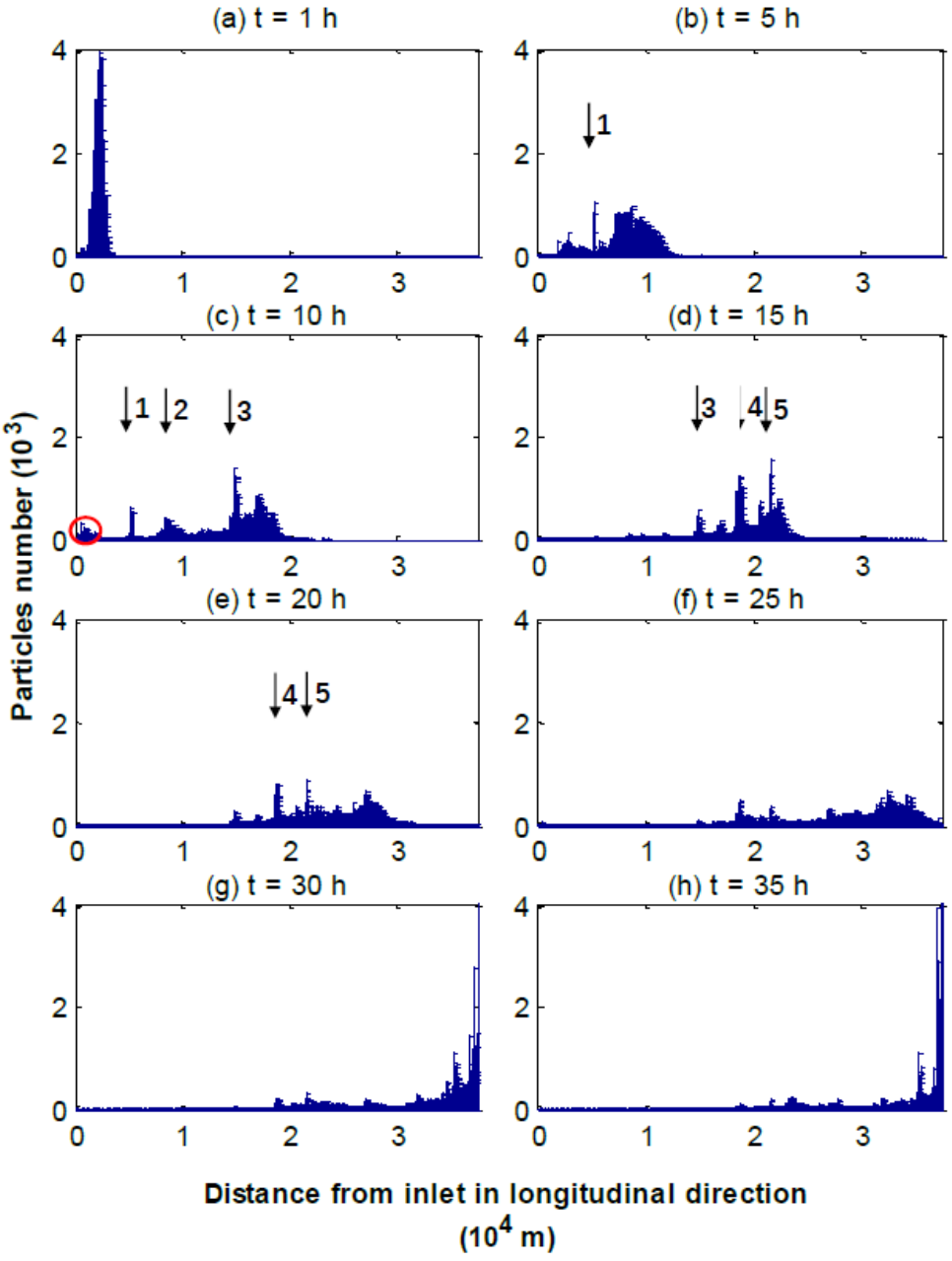

Fig. 13 Longitudinal particles concentration profile development at t = 1, 5, 10, 15, 20, 25, 30, 35h

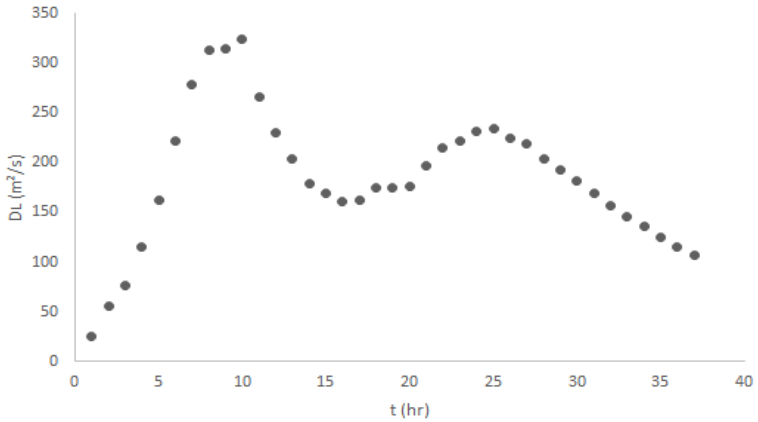

.

Fig. 14 Development of DL with time at the Three Gorges area in Yangtze river

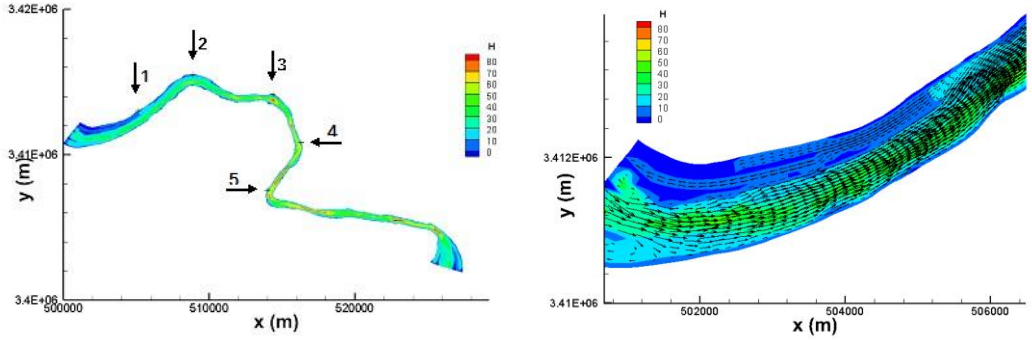

(a) Locations at the river where the odd points occur in the concentration profiles

(b) The back-flow at the front part of the river which leading to the first odd peak in concentration and the travel-back of some particles

Fig. 15 Explanation figures for the odd points in the concentration development

5.2 Estimate D_L by empirical/theoretical formulae

Due to the lack of field data, empirical or theoretical formulae are applied to estimate the longitudinal dispersion coefficient D_L. In this section, D_L simulated by the random walk model above is verified against that calculated by empirical or theoretical formulae.

From 70s of last century, several empirical or theoretical formulae for D_L have been introduced for natural rivers [15][24][25][26][27][28][29]. Due to the complexity of natural rivers (shape irregularity, vegetations and dead zones), the longitudinal dispersion coefficient does not have a complete theoretical predictor. Fisher [13] first investigated D_L in natural rivers and found that D_L is mainly caused by the depth-averaged velocity gradient in the transverse direction because of the large width-to-depth ration in natural rivers. Thereafter, similar studies have been conducted [24][30]. These are the most widely used type of formulae for D_L, and we select Fisher's formula as a classic representative:

$$D_L = 0.011\frac{\bar{u}^2 W^2}{du_*} \tag{13}$$

where the flow velocity u, river width W, flow depth d and shear velocity u_* are taken as their average values along the river, respectively. Thenceforth, by using many measured data sets, Fischer [15] found that the D_L for some natural rivers have a hugely wide range, as $D_L/d\,u_*$ varying from 8.6 to 7500, which generally being much greater than Elder's [31] equation constant of 5.93 in Eq. (2). Elder underestimated the dispersion coefficients significantly mainly due to the exclusion of transverse variation in the velocity profile across the natural rivers.

It is noted that in the formulae of this type [15][24][30], D_L is inversely proportional to $d\,u_*$. However, the latter formulae show D_L being proportional to $d\,u_*$ [25][28][32][33]. Therefore, we select another representative from this category of formulae. It is worth mentioning that these formulae are based on the precondition of large width-height ratio (average value of W/d is 72.7 [29]). However, the ratio of width to depth for the reach at the Yangtze River is W/d =17.69. Hence Etemad's [28] formula was chosen because it gave a classified discussion according to the width-height ratio:

$$D_L = \begin{cases} 15.49(W/d)^{0.78}(U/u_*)^{0.11}du_*, & \text{if } W/d \le 30.6 \\ 14.12(W/d)^{0.61}(U/u_*)^{0.85}du_*, & \text{if } W/d \ge 30.6 \end{cases} \tag{14}$$

The ratio of width to depth for the reach at Yangtze River is smaller than 30.6, thus the first formula is applied and D_L =*119.20*.

Besides, Wang [29] recently proposed a canonical form for D_L that better reflects the physics of dispersion and suits complex flow conditions encountered in natural streams.

$$D_L = \eta U R_d \quad (15)$$

Where $\eta = 47.9d/W + 0.718$ for natural rivers. R_d is defined as the major lateral scale. R_d for the Yangzte river, where the width is much larger than the depth, can be regarded as its width. As most exponents of physical formulae are integers, Wang's formula seems physically sound compared with the form of the formulae in previous studies. Hence it is also selected for comparison.

Finally, the longitudinal dispersion coefficient D_L that is estimated by these formulae are compared with that by the random walk model, as shown in Table.1

Table 1 Longitudinal dispersion coefficient estimated by empirical equations and random walk model

d (m)	*U (m/s)*	*W(m)*	*u∗* (m/s)	D_L (m^2/s)			
				Fischer[15]	Etemad[28]	Wang[29]	random walk
34.71	0.26	614.09	1.75E-02	473.72	119.20	553.23	207.34

It is also mentionable that many critical assumptions in the derivation of these empirical equations cannot stand in the natural environment, consequently the results are not very reliable. The results of these formulae may differ significantly with the measured data, with the difference up to four times [34][35]. Considering the measured data can also be two times different against the true values, it is acceptable as long as the difference between the D_L by these formulae and that by the random walk model is under four times range. Hence the estimation of D_L by the random walk model is valid and in acceptable level of accuracy.

Besides, the random walk method presents the development of the longitudinal dispersion coefficient along with particles travel time. Hence the variation of the river topography that the particles pass by can also be reflected. On the other hand, all the formulae for the prediction of D_L is a rough average along the river. Besides, the variation of D_L along with time always land into reasonable values, compared with that by formulae, which can prove the validity of the random walk model.

Because of the unreliability presented above, further studies are needed in the future for such complex natural cases. As known by all, the Three Gorges Project, as well as the Gezhouba Dam, span over the Yangtze River and a huge reservoir. The former one can be treated as the depth-averaged two-dimensional case. While the latter case, the reservoir, which has a large area as well as a deep depth in some area, needs much more complicated treatment. The three-dimensional study might be necessary in such analysis, demanding a different calculation scheme for the three-dimension environment. Furthermore, vegetation, sediment etc. should be taken into consideration. In summary, more complicated treatment should be applied to this natural environment in future studies in order to obtain a higher level of accuracy.

6. Summary

The random walk model is applied to solve the depth-integrated advection/diffusion/decay equation. Also, the TVD-Mac model, as a representative of Eulerian method, is used for the same simulation to compare with the random walk model

First, both numerical models have been tested by two idealized cases, for which analytical solutions exist. For pure advection scenario with or without decay, numerical dissipation is observed for TVD-Mac model, where the concentration changes abruptly. On the contrary, the RWPT enjoys no numerical dissipation at anywhere, and stays much closer to the analytical solution. The same advantages of RWPT present when dealing with the uniform flow with both advection and diffusion. The Eulerian method can simulate the x-direction flow as accurate as RWPT. However, when disalignment appears between the flow direction and grid orientation, the relative errors of TVD-Mac model go much higher. On the other hand, simulations by RWPT achieve much higher accuracy for both cases with almost no numerical dissipation. It is also worth mentioning that the random walk model can handle the case with cross-diffusion term with the same accuracy as that without such disalignment.

Through a test on the solute oscillation along a one-dimensional hypothetical estuary, the present random walk model is demonstrated to have the advantage of accurately conserving mass and less numerical diffusion as the solute moves back and forth with the tide. Such advantage is highlighted through the comparison with the simulations by two Eularian method, the TVD-Mac model which conserves mass better while suffers from larger numerical diffusion, and the DIVAST model which has less numerical diffusion but a fluctuation on total mass.

Finally, the model has been applied to study a pollutant transportation case in a natural scenario: the reach of the Yangtze River. Thanks to the work by Liang ([14]), the flow velocity fields as well as water depth at the reach of Yangtze River are already known, thus can be used by RWPT as the input condition. A large number of particles are tracked by the random walk model, and the longitudinal dispersion coefficient D_L is calculated through statistical analysis on particles resemble. Several empirical/theoretical formulae are selected to estimate D_L in nature rivers and compare with that by RWPT. Again, reasonably good agreement is achieved, demonstrating the validation of the random walk model in solving complex real-world problems.

References

[1] Rajar, R., The role of mathematical models, physical models and field measurements in water pollution problems. Proc. of the 4th Int. Conf. on Water Pollution, Computational Mechanics Publications: Southampton, UK, pp. 545-555, 1997.

[2] Dortch, M.S., Advances in water quality modeling in the coastal environment. Advances in Coastal Modeling, ed. V.C. Lakhan, Elsevier Science: Amsterdam, pp. 491-503, 2003.

[3] Liang, D., Falconer, R.A., Lin, B., 2006. Comparison between TVD-MacCormack and ADI-type solvers of the shallow water equations. Advances in Water Resources 29 (12), 1833e1845.

[4] Mingham, C.G., et. al, 2001. A TVD MacCormack scheme for transcritical flow. Proceedings of the Institute of Civil Engineers e Water and Maritime Engineering 148 (3), 167e175.

[5] Peter Salamon, et. al, A review and numerical assessment of the random walk particle tracking method, Journal of Contaminant Hydrology, Volume 87, Issues 3–4, 2006, pp 277-305

[6] Bram van Leer, Towards the ultimate conservative difference scheme. A second-order sequel to Godunov's method, In Journal of Computational Physics, V 32, Issue 1, 1979, P 101-136,

[7] Benkhaldoun, F., Elmahi, I., et al. (2007). Well-balanced finite volume schemes for pollutant transport by shallow water equations on unstructured meshes. Journal of Computational Physics, 226(1):180–203.

[8] Liang, D., Lin, B., and Falconer, R. (2007). Simulation of rapidly varying flow using an efficient TVD-MacCormack scheme. International Journal for Numerical Methods in Fluids, 53(5):811–826.

[9] Liu ZW(*), Chen YC, Zhu DJ. Study on the Concentration Distribution in a Trapezoidal Open-Channel Flow with a side Discharge. Environmental Fluid Mechanics, 2007, 7(6): 509-517.

[10] Liu ZW(*), Chen YC, Li L, Zheng JY. Sigma-coordinate Numerical Model for Side-discharge into Natural Rivers. Journal of Hydrodynamics, 2009, 21(3):333-340.

[11] Liang, D. and Xuefei, W.U., 2014. A random walk simulation of scalar mixing in flows through submerged vegetations. Journal of Hydrodynamics, Ser. B, 26(3), pp.343-350.

[12] Barber, R. and Volakos, N. (2005). Modelling depth-integrated pollution dispersion in the Gulf of Thermaikos using a Lagrangian particle technique. WIT Transactions on Ecology and the Environment, 80:173–184.

[13] Periáñez, R. (2004). A particle-tracking model for simulating pollutant dispersion in the Strait of Gibraltar. Marine Pollution Bulletin, 49(7-8):613–23.

[14] Liang, D.,Wang, X., Falconer, R., and Bockelmann-Evans, B. (2010). Solving the depth-integrated solute transport equation with a TVD-MacCormack scheme. Environmental Modelling & Software, 25(12):1619–1629

[15] Fischer, H. (1973). Longitudinal dispersion and turbulent mixing in open-channel flow. Annual Review of Fluid Mechanics, 5(1):59–78.

[16] Józsa, J. (1989). 2D particle model for predicting depth-integrated pollutant and surface oil slick transport in rivers. In Proc. of the 1st Int. Conf. on Hydraulic and Environmental Modelling of Coastal, Estuarine and River Waters, pages 332–340.

[17] Kinzelbach,W., 1987. The RWPT in pollutant transport simulation. Advances in analytical and

numerical groundwater flow and quality modelling. In: Custodio, E., et al. (Eds.), NATO ASI Series C, vol. 224, pp. 227–246.
[18] Xuefei Wu, Dongfang Liang, On the Accuracy of the Random Walk Simulation of Pollu- tant Dispersion, Second Conference of Global Chinese Scholars on Hydrodynamics, 2016
[19] Balzano, A. (1998). Evaluation of methods for numerical simulation of wetting and drying in shallow water flow models. Coastal Engineering, 34(1):83–107.
[20] Lin, B. and Falconer, R. A. (1997). Tidal flow and transport modeling using ULTIMATE QUICKEST scheme. Journal of Hydraulic Engineering, 123(4):303–314.
[21] Carroll,W. (2007). In consideration of Thames Outer Barrier. Master's thesis, University of Cambridge.
[22] Ye, L., et, al. (2009). The influence of topography and land use on water quality of Xiangxi River in Three Gorges Reservoir region. Environmental Geology, 58(5):937–942.
[23] Scholz-Starke, B., et al. (2013). An integrated approach to model the biomagnification of organic pollutants in aquatic food webs of the Yangtze Three Gorges Reservoir ecosystem using adapted pollution scenarios. Environmental Science and Pollution Research, P1–18.
[24] Liu, H. (1977). Predicting dispersion coefficient of streams. In Journal of the Environmental Engineering Division, American Society of Civil Engineers, volume 103.
[25] Seo, I. W. and Cheong, T. S. (1998). Predicting longitudinal dispersion coefficient in natural streams. Journal of Hydraulic Engineering, 124(1):25–32.
[26] Kashefipour, S. M. and Falconer, R. A. (2002). Longitudinal dispersion coefficients in natural channels. Water Research, 36(6):1596–1608.
[27] Fuat Toprak, Z. and Savci, M. E. (2007). Longitudinal dispersion coefficient modeling in natural channels using fuzzy logic. Clean–Soil, Air, Water, 35(6):626–637.
[28] Etemad-Shahidi, A., Taghipour, M., 2012. Predicting longitudinal dispersion coefficient in natural streams using M5' model tree. J. Hydraulic Eng. 138 (6), 542–554.
[29] Wang YF, Huai WX, Wang WJ. Physically sound formula for longitudinal dispersion coefficients of natural rivers. Journal of Hydrology. 2017 Jan 31;544:511-23.
[30] Bogle, G.V., 1997. Stream velocity profiles and longitudinal dispersion. J. Hydraulic Eng. 123 (9), 816–820.
[31] Elder, J. (1959). The dispersion of marked fluid in turbulent shear flow. Journal of Fluid Mechanics, 5(04):544–560.
[32] Li, X., Liu, H., Yin, M., 2013. Differential evolution for prediction of longitudinal dispersion coefficients in natural streams. Water Resour. Manage 27 (15), 5245–5260.
[33] Sattar, A.M., Gharabaghi, B., 2015. Gene expression models for prediction of longitudinal dispersion coefficient in streams. J. Hydrol. 524, 587–596.
[34] Changzhao, Y. (1992). Introduction to Environmental Fluid Dynamics. Tsinghua University Press.
[35] Toprak, Z. F. and Cigizoglu, H. K. (2008). Predicting longitudinal dispersion coefficient in natural streams by artificial intelligence methods. Hydrological Processes, 22(20):4106–4129.